# Watt-Level Dual-Wavelength Q-Switched Mode-Locked All-Solid-State Tm:CYA Laser

Chen Chen [1,2], Weijun Ling [1*], Rui Sun [1,3], Qiang Xu [2,3*] and Yani Zhang [2,3]

[1] Institute of Laser Technology, Tianshui Normal University, Tianshui, China, [2] Baoji Engineering Technology Research Center on Ultrafast Laser and New Materials, Baoji, China, [3] School of Physics and Optoelectronics Technology, Baoji University of Arts and Science, Baoji, China

A passively Q-switched mode-locked all-solid-state Tm:CaYAlO$_4$ (Tm:CYA) laser with a MoS$_2$ saturable absorber is demonstrated for the first time. Employing a typical X-type cavity and output coupling mirror of 9%, when the laser diode pump power is higher than 8.5 W, the laser enters into a stable Q-switched mode-locked operation, further increasing the pump power into a dual-wavelength operating state; the corresponding typical center wavelengths are 1,863 and 1,877 nm. When the pump power reaches 20 W, the maximum output power is 1.15 W, the frequency of mode-locked pulse is 103.7 MHz, and the modulation depth of mode-locked pulses in the Q envelope is close to 100%. The results prove that MoS$_2$ saturable absorber is suitable for 2-μm high-power mode locking.

Keywords: Tm:CYA laser, MoS$_2$ saturable absorber, Q-switching and mode-locking, dual wavelength, diode pumped

## INTRODUCTION

The 2-μm band is located at the absorption peak of water and the window band of atmosphere, which is a safe area for the human eye. Based on the above characteristics, 2 μm band laser is widely used in high-precision surgery [1], free space communication [2], and other fields. In particular, high-power dual-wavelength mode-locked lasers can generate coherent terahertz radiation by difference frequency [3, 4], which is widely used in differential radar and remote space detection [5].

Passive mode locking is one of the common methods to obtain ultrashort pulse. In general, the mode-locked technique needs to have saturable absorber (SA), non-linear loop mirror, or non-linear polarization rotating [6]. At present, many materials have been employed as SA for passively mode-locked lasers, such as semiconductor saturable absorption mirrors, carbon nanotubes, graphene, and black phosphorus [7, 8]. An excellent SA should possess the properties of higher damage threshold, ultrafast recovery time, and lower saturation intensity [9, 10]. Among them, due to the complex process, narrow working bandwidth, and high cost of semiconductor saturable absorption mirrors, we need to look for other materials. Carbon nanotubes are widely used in fiber lasers [11, 12], but their performance is poor in 2 μm solid-state lasers due to their unique structures and properties. Graphene is widely used in 1 μm, but its absorption efficiency at 2 μm is weak, which limits its ability to adjust light, and black phosphorus is easily oxidized in the presence of oxygen and water, leading to its instability in the experiment [13]. As such, MoS$_2$ has attracted our attention with its universality and good stability. MoS2, as a SA, was first widely used in fiber lasers [14–16]. Later, it is slowly used in solid-state lasers to realize Q-switching or mode-locked operation. In 2015, a passively Q-switched mode-locked (QML) Tm:LiLuF4 (LLF)

laser with a MoS2 SA is demonstrated for the first time [17]. In 2017, the maximum peak power of 4.33 W is obtained using $MoS_2$ as SA in Er:LUAG laser [18]. Next year, Li et al. first used $MoS_2$ to realize Q-switched operation and obtained an average output power of 3.3 W in Tm,Ho:YAP lasers [19]. We also use $MoS_2$ SA to realize QML operation in Tm,Ho:LLF [20] and Tm:LuAG [21] lasers, respectively. In short, $MoS_2$ has great potentiality according to the current experimental progress.

CYA crystals are widely used because of their excellent mechanical strength, chemical stability, and high thermal conductivity [22]. As early as 1997, Tm:CYA crystal was pumped by Ti:Sapphire laser to realize continuous wave (CW) operation, in which the output power and slope efficiency were 50 mW and 18%, respectively [23]. In 2015, Kong et al. demonstrated a CW mode-locked Tm:CYA laser with a maximum output power of 830 mW and obtained dual-wavelength output of 1,958.9 and 1960.6 nm [24]. The next year, Yao et al. pumped Tm:CYA with a Raman fiber laser and obtained output of up to 6.8 W under CW operation [25]. Recently, Lan et al. used $MoS_2$ for the first time to achieve Q-switched operation in Tm:CYA laser, with the maximum output power of 0.49 W [26].

In this paper, we first use $MoS_2$ as SA to realize a Watt-level dual-wavelength QML operation in Tm:CYA laser. The output power of QML laser is 1.153 W, and the dual-wavelength is 1,863 and 1,877 nm, respectively. The dual-wavelength laser will have a broad application prospect in the field of optical communication and sensing.

## PREPARATION OF MOS$_2$ SA

In this experiment, $MoS_2$ SA is prepared by liquid phase stripping method. First, the powdered $MoS_2$ is added to the water-based solution with a concentration of ~1 mg/ml. Then, a glass substrate is prepared by the following procedure. First, the glass substrate is immersed in deionized water. Second, it is treated with ultrasonic cleaning apparatus for ~10 min. Third, the surface dust of substrate is removed by ultrasound in alcohol for 10 min. Fourth, the treated glass piece is placed in a mixed solution of sulfuric acid and hydrogen peroxide for ~1 h before hydrophilic treatment. Finally, the glass piece is soaked in the glass in clean deionized water for ~10 min. Then, the glass substrate is prepared, and then the prepared $MoS_2$ solution was dropped on it directly. **Figure 1a** is the electron micrograph of $MoS_2$, which proves that $MoS_2$ has been spun on the glass substrate. **Figure 1b** shows the Raman spectrum of $MoS_2$. The phonon vibration modes of $MoS_2$ mainly include $E^1_{2g}$ (in plane) and $A_{1g}$ (out of plane), and the two main vibration modes change with the thickness. Specifically, the $A_{1g}$ mode shifted blue, while
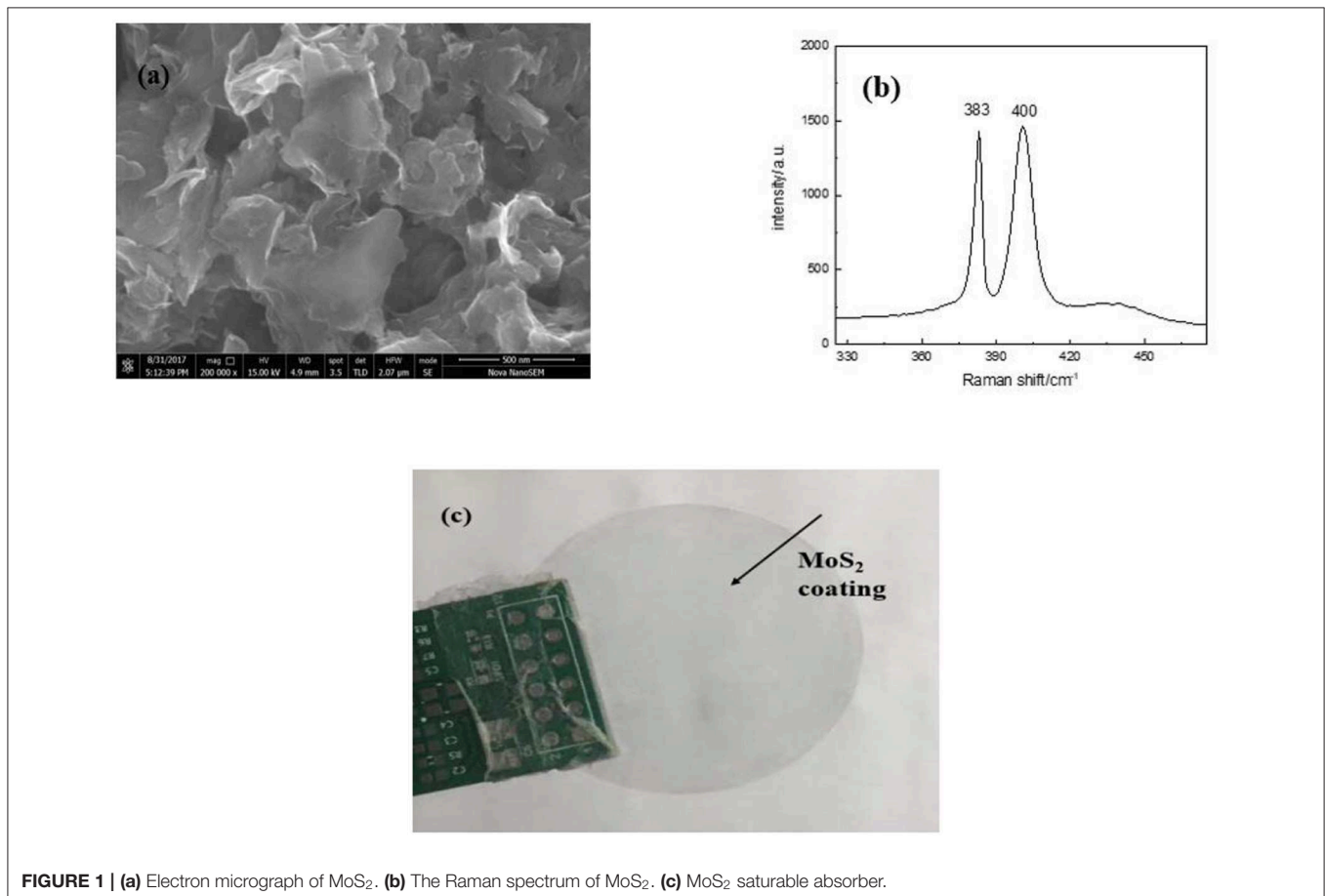


FIGURE 1 | (a) Electron micrograph of $MoS_2$. (b) The Raman spectrum of $MoS_2$. (c) $MoS_2$ saturable absorber.
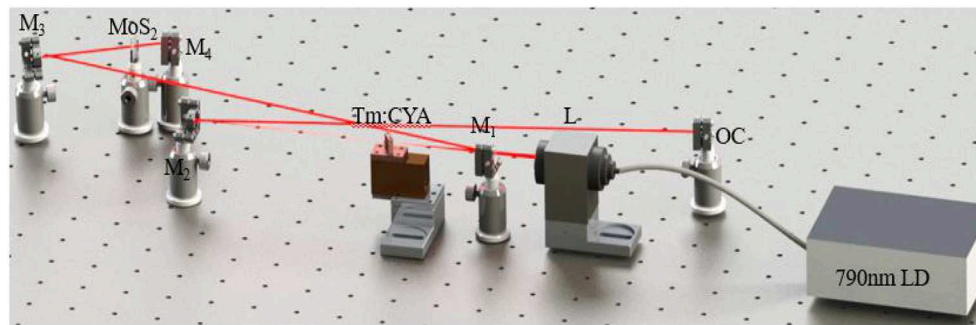
FIGURE 2 | The experiment setup of dual-wavelength Q-switched mode-locked Tm:CYA laser.

the $E_{2g}$ mode shifted red. In the figure, $E_{2g}$ and $A_{1g}$ are located at 383 and 402 cm$^{-1}$, respectively. It can be seen that MoS$_2$ is a small layer structure indeed. The prepared MoS$_2$ SA material is shown in **Figure 1c**.

## EXPERIMENTAL SETUP

The experiment setup of dual-wavelength QML Tm:CYA laser is shown in **Figure 2**. In this experiment, a 790 nm laser diode (LD) with a maximum output power of 30 W is used as the pump source. The Tm:CYA crystal is cut at the Brewster angle, and the two end faces are polished. The doped concentration of Tm$^{3+}$ is 4%, and the size is $3.8 \times 4 \times 4$ mm. The crystal was wrapped with indium foil and tightly mounted in a water-cooled copper block system with stable temperature holding at 11°C. L is the pump focusing and collimating system with a ratio of 1:0.8 and a transmittance of 95% for 790 nm. Its working distance is 49.2 mm, and external diameter is 37.5 mm. In the laser cavity, M1 and M2 are flat concave mirrors with curvature radius of 75 and 100 mm, respectively. Both have high transmissivity to pump light and highly reflective to 1,850–2,100 nm. M3 is a flat-concave mirror with a curvature radius of 100 mm and has a reflectivity of more than 99.9% for wavelength from 1,850 to 2,100 nm, whose main function is to focus the oscillating light to the SA and start QML operation. M4 is a flat mirror with the same reflective film as M3. In the experiment, plane mirrors with 3, 5, and 9% transmissivity are used as the output couplers (OC).

## EXPERIMENTAL RESULTS AND DISCUSSION

The output power as a function of the pump power is plotted in **Figure 2**. Contrast experiments are carried out with OCs with different transmissivities of 3, 5, and 9%, respectively. At first, the CW laser performance is discussed without MOS$_2$ SA in the cavity. The threshold power of 3% OC is 2.4 W, the slope efficiency is 11%, and the maximum output power of 1,857 mW is obtained at 20 W pump power. The threshold power of 5 and 9% OC are 2.6 and 2.8 W, respectively. When pump power is 20 W, the maximum output power is increased to 2,380 and 2,600 mW, respectively. To obtain high power output, we theoretically
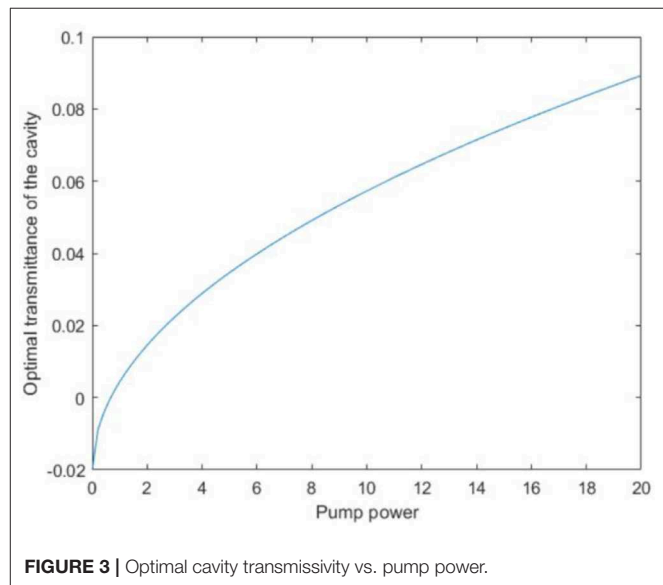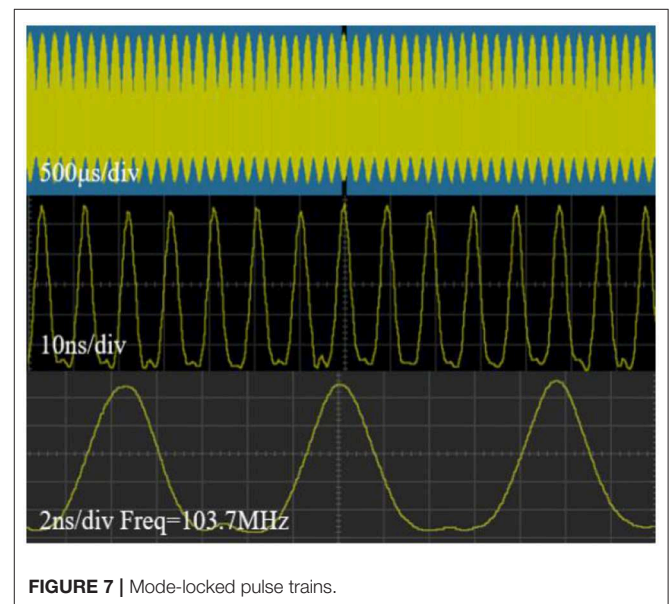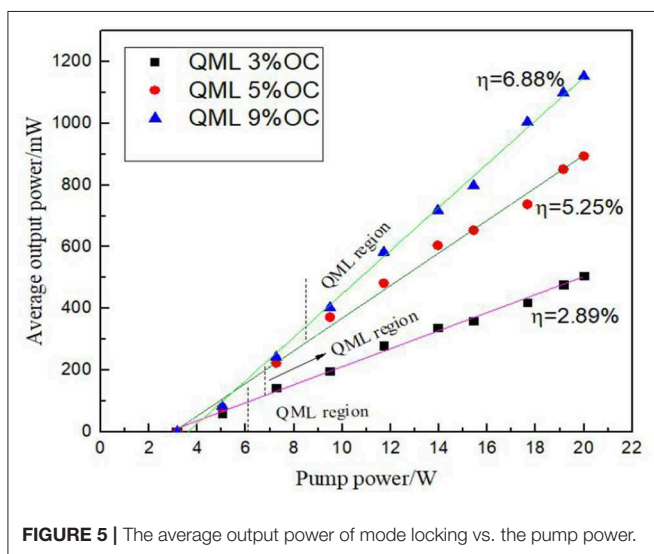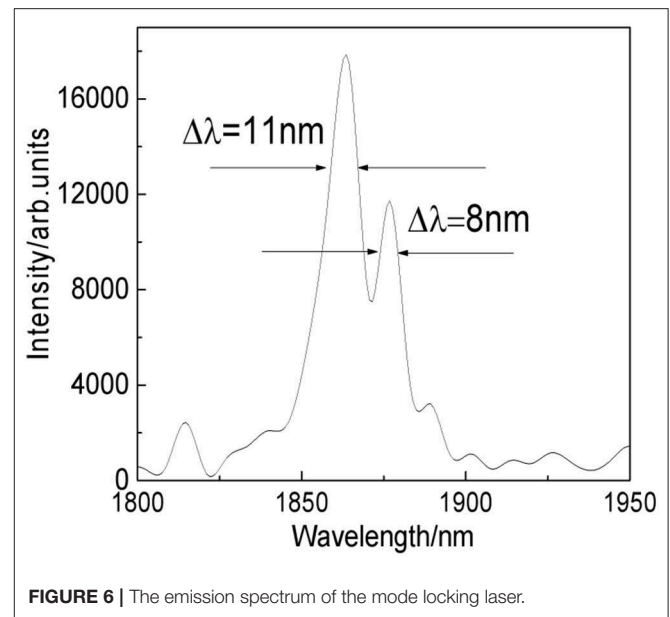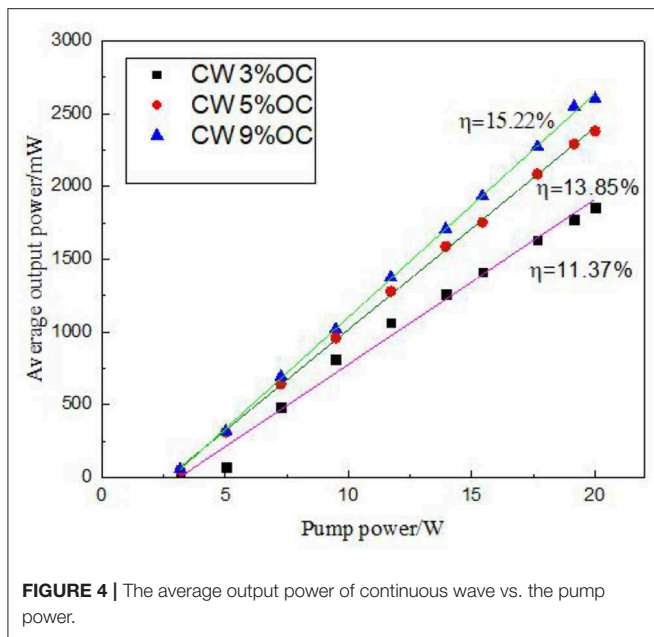


FIGURE 3 | Optimal cavity transmissivity vs. pump power.

simulate the optimal transmissivity parameters of the OC.

$$T = \sqrt{\frac{4\sigma \tau_f \lambda_P P_{in} \left[1 - \exp\left(1 - \alpha_p L\right)\right] \times \delta_0}{\pi h c \left(\overline{W_P}^2 + W_0^2\right)}} - \delta_0 \quad (1)$$

The relationship between the best transmissivity of the cavity and the pump power is shown in Equation (1), where $\sigma$ is the crystal emission cross-section, $\tau_f$ is the emission life, $\lambda_P$ is the pump wavelength, $P_{in}$ is the pump power, $\alpha_p$ is absorption coefficient, $L$ is the crystal length, $\delta_O$ is the cavity loss, $\overline{W_P}$ is the average pump spot radius, and $W_O$ is the oscillating spot radius. Through the simulation Equation (1), the curve of **Figure 3** is obtained. It can be seen from the figure that when the pump power is 20 W, the optimal transmissivity $T$ of the cavity is ∼0.088. Considering the actual situation of optical glass coating in processing, it is more appropriate to choose an output mirror with a transmittance of 0.09.

When the MoS$_2$ SA is inserted into the cavity, the laser oscillation is obtained with the threshold power of 3, 3.2, and

FIGURE 4 | The average output power of continuous wave vs. the pump power.



FIGURE 6 | The emission spectrum of the mode locking laser.



FIGURE 5 | The average output power of mode locking vs. the pump power.



FIGURE 7 | Mode-locked pulse trains.

3.5 W under 3, 5, and 9% OC, respectively. After entering the stable QML operation, the corresponding maximum output power is 506, 894, and 1,153 mW. The relationship between average output power and pump power in CW and QML operation is shown in **Figures 4**, **5**, respectively. Through the comparison of the different OCs mentioned above, it is found that the QML output power of 9% OC is up to 1.15 W, which is the highest output power among all OCs. This is also consistent with the theoretical simulation above. This kind of QML pulse has potential application in remote detection.

The spectrum of the QML pulse is measured using an optical spectrum analyzer (AvaSpec-NIR256-2.5 TEC). As shown in **Figure 6**, the dual-wavelength synchronous output is obtained with the center wavelength of 1,863 and 1,877 nm and the

spectrum of half-width of 11 and 8 nm, respectively. It is found that the central wavelength and the spectral width of the spectrum do not change with the output power, and the output spectrum is stable.

The pulses of QML laser were recorded by a fast photodiode (ET-500) with a digital oscilloscope (RIGOL, DS4034). The typical QML pulse trains in 500 μs, 10 ns, and 2 ns timescales are shown in **Figure 7**. The QML pulses have a repetition frequency of 103.7 MHz, corresponding to the laser cavity length of 1.45 m.

Since the autocorrelator is only suitable for measuring the pulse width of CW mode-locked pulse, the Q-switched mode-locked pulse cannot obtain autocorrelation envelope because of the envelope modulation of kilohertz, so we can only estimate

the pulse duration roughly in theory. Here, Equation (2) is used to estimate the width of the QML pulse [27].

$$t_m = \sqrt{t_r^2 + t_p^2 + t_o^2} \tag{2}$$

Here, $t_m$ is the rising edge time of the measured mode-locked pulse, $t_r$ is the rising edge time of the actual mode-locked pulse, $t_p$ is the rising edge time of the photodetector, and $t_o$ is the rising edge time of the oscilloscope. In the experiment, the rising edge time of the mode-locked pulse is ~2.06 ns, and the rising edge time of the photodetector is ~35 ps. $t_o$ can be estimated as 1,900 ps using the Equation (2) as follows.

$$t_0 \times W_b = 0.35 \sim 0.4 \tag{3}$$

Among them, $W_b$ is the bandwidth of the oscilloscope, which is 200 MHz in the experiment. Thus, it can be calculated that the rise time of the mode-locked pulse is ~795 ps. Since the actual mode-locked pulse width is ~1.25 times of the rising edge time, it is calculated as 994 ps.

## CONCLUSION

In conclusion, we first use $MoS_2$ SA to realize a Watt-level dual-wavelength Q-switched mode locked operation in the Tm:CYA laser. Using a typical "X" type five mirror folded cavity, a maximum CW output power of 2.6 W is obtained under 9% output coupling mirror. After the laser enters into stable dual-wavelength QML operation, the maximum output power reaches 1.15 W with central wavelengths of 1,863 and 1,877 nm. The repetition frequency of QML is 103.7 MHz, and the modulation depth of mode-locked pulses in the Q envelope is close to 100%. The results show that $MoS_2$ SA is suitable for $2\,\mu m$ high-power mode locking and has potential application value in high-power mode locking. Next step, we will strive to achieve high-power CW mode-locked operation by increasing the pump power and reducing the loss of $MoS_2$. The LD pumped high-power mode-locked laser has the advantage of low cost and will be widely used in industrial production.

## DATA AVAILABILITY STATEMENT

All datasets generated for this study are included in the article/supplementary material.

## AUTHOR CONTRIBUTIONS

WL and QX designed the overall scheme. CC and RS carried out specific experiments. YZ provided experimental guidance.

## FUNDING

## REFERENCES

1. Wang J, Sramek C, Paulus YM, Lavinsky D, Schuele G, Anderson D, et al. Retinal safety of near-infrared lasers in cataract surgery. *J Biomed Optics.* (2012) **17**:95001. doi: 10.1117/1.JBO.17.9.095001

2. Chan VWS. Optical space communications. *IEEE J Select Topics Quant Electr.* (2000) **6**:959–75. doi: 10.1109/2944.902144

3. Majkic A, Zgonik M, Petelin A, Jazbinsek M, Ruiz B, Medrano B, et al. Terahertz source at 9.4 THz based on a dual-wavelength infrared laser and quasi-phase matching in organic crystals OH1. *Appl Phys Lett.* (2014) **105**:141115. doi: 10.1063/1.4897639

4. Chang JH, Wang TT, Zhang C, Zhang C, Ge YX, Tao ZH. Compact and tunable mid-IR light source based on a dual-wavelength fiber laser. *Chin Phys Lett.* (2013) **30**:114206. doi: 10.1088/0256-307X/30/11/1 14206

5. Walsh BM. Review of Tm and Ho materials; spectroscopy and lasers. *Laser Phys.* (2009) **19**:855–66. doi: 10.1134/S1054660X09040446

6. Liu XM. Hysteresis phenomena and multipulse formation of a dissipative system in a passively mode-locked fiber laser. *Phys Rev A.* (2010) **81**:023811. doi: 10.1103/PhysRevA.81.023811

7. Liu XM, Popa D, Akhmediev N. Revealing the transition dynamics from Q Switching to mode locking in a soliton laser. *Phys Rev Lett.* (2019) **123**:093901. doi: 10.1103/PhysRevLett.123.093901

8. Liu XM, Yao XK, Cui YD. Real-time observation of the buildup of soliton molecules. *Phys Rev Lett.* (2018) **121**:023905. doi: 10.1103/PhysRevLett.121.023905

9. Kong LC, Xie GQ, Yuan P, Qian LJ, Wang H, Yu H, et al. Passive Q-switching and Q-switched mode-locking operations of $2\,\mu m$ Tm: CLNGG

laser with $MoS_2$ saturable absorber mirror. *Photon Res.* (2015) **3**:A47–50. doi: 10.1364/PRJ.3.000A47

10. Guo B. 2D noncarbon materials-based nonlinear optical devices for ultrafast photonics. *Chin Optics Lett.* (2018) **16**:020004. doi: 10.3788/COL201816.020004

11. Liu XM, Pang M. Revealing the buildup dynamics of harmonic mode-locking states in ultrafast lasers. *Laser Photon Rev.* (2019) **13**:1800333. doi: 10.1002/lpor.201800333

12. Liu XM, Han DD, Sun ZP, Zeng C, Lu H, Mao D, et al. Versatile multi-wavelength ultrafast fiber laser mode-locked by carbon nanotubes. *Sci Rep.* (2013) **3**:2718. doi: 10.1038/srep02718

13. Sun XL, Nie HK, He JL, Zhao RW, Su XC, Wang YR, et al. Passively mode-locked $1.34\,\mu m$ bulk laser based on few-layer black phosphorus saturable absorber. *Opt Express.* (2017) **25**:20025–32. doi: 10.1364/OE.25.020025

14. Du J, Wang Q, Jiang G, Xu CW, Zhao CJ, Xiang YJ, et al. Ytterbium-doped fiber laser passively mode locked by few-layer Molybdenum Disulfide ($MoS_2$) saturable absorber functioned with evanescent field interaction. *Sci Rep.* (2014) **4**:6346–9. doi: 10.1038/srep06346

15. Luo ZQ, Huang YZ, Zhong M, Li YY, Wu JY, Xu B, et al. 1-, 1.5-, and $2\text{-}\mu m$ fiber lasers q-switched by a broadband few-layer mos2 saturable absorber. *J Light Technol.* (2014) **32**:4077–84. doi: 10.1109/JLT.2014.2362147

16. Du TJ, Luo ZQ, Yang RH, Huang YZ, Ruan QJ, Cai ZP, et al. 1.2-W average-power, 700-W peak-power, 100-ps dissipative soliton resonance in a compact Er:Yb co-doped double-clad fiber laser. *Optics Lett.* (2017) **42**:462–5. doi: 10.1364/OL.42.000462

17. Zou X, Leng YX, Li YY, Feng YY, Zhang PX, Hang Y, et al. Passively Q-switched mode-locked Tm:LLF laser with a MoS2 saturable absorber. *Chin Opt Lett.* (2015) **13**:081405. doi: 10.3788/COL201513.081405

18. Zhang SY, Guo L, Fan MQ, Lou F, Gao P, Hao L, et al. Passively Q-switched Er:LuAG laser at 1.65 $\mu$m using MoS$_2$ and WS$_2$ saturable absorbers. *IEEE Photon J.* (2017) **9**:1–7. doi: 10.1109/JPHOT.2017.2691740

19. Li LJ, Yang XN, Zhou L, Xie WQ, Wang YL, Shen YJ, et al. Active/passive Q-switching operation of 2 $\mu$m Tm,Ho:YAP laser with an acousto-optical Q-switch/MoS2 saturable absorber mirror. *Photon Res.* (2018) **6**:614–9. doi: 10.1364/PRJ.6.000614

20. Ling WJ, Xia T, Dong Z, Zuo YY, Li K, You LF, et al. Passively Q-switched mode-locked Tm,Ho:LLF laser with a reflection-type MoS$_2$ saturable absorber. In: *International Conference on Optical Instruments and Technology: Advanced Laser Technology and Applications.* Beijing (2018), p. 106190Q. doi: 10.1117/12.2295490

21. Ling WJ, Sun R, Chen C, Zhang YN, Kang CP, Xu Q, et al. Passively Q-switched mode-locked Tm:LuAG laser with reflective MoS$_2$ saturable absorber. *Chin J Lasers.* (2019) **46**:0808002. doi: 10.3788/CJL201946.0808002

22. Kustov EF, Petrov VP, Petrova DS, Udalov JP. Absorption and luminescence spectra of Nd$^{3\pm}$ and Er$^{3\pm}$ ions in monocrystals of CaYAlO$_4$. *Phys Status Solid.* (1977) **41**:379–83. doi: 10.1002/pssa.2210410204

23. Moncorgé R, Garnier N, Kerbrat P, Wyon C, Borel C. Spectroscopic investigation and two-micron laser performance of Tm$^{3+}$:CaYAlO$_4$ single crystals. *Opt Commun.* (1997) **141**:29–34. doi: 10.1016/S0030-4018(97)00219-8

24. Kong LC, Qin ZP, Xie GQ, Xu XD, Xu J, Yuan P, et al. Dual-wavelength synchronous operation of a mode-locked 2-$\mu$m Tm: CaYAlO$_4$ laser. *Opt Lett.* (2015) **40**:356–8. doi: 10.1364/OL.40.000356

25. Yao WC, Wu F, Zhao YG, Chen H, Xu XD, Shen DY. Highly efficient Tm:CaYAlO$_4$ laser in-band pumped by a Raman fiber laser at 1.7 $\mu$m. *Appl Opt.* (2016) **55**:3730–3. doi: 10.1364/AO.55.003730

26. Lan JL, Zhang XY, Zhou ZY, Xu B, Xu HY, Cai ZP, et al. Passively Q-switched Tm:CaYAlO$_4$ laser using a MoS$_2$ saturable absorber. *IEEE Photon Technol Lett.* (2017) **29**:515–9. doi: 10.1109/LPT.2017.2662699

27. Li ZY, Zhang BT, Yang JF, He JL, Huang HT, Zuo CH, et al. Diode-pumped simultaneously Q-switched and mode-locked Nd:GdVO$_4$/LBO red Laser. *Laser Phys.* (2010) **20**:761–5. doi: 10.1134/S1054660X10070170